# Crystal structure of extracellular domain of human lectin-like transcript 1 (LLT1), the ligand for natural killer receptor-P1A

Shunsuke Kita[1, †], Haruki Matsubara[1, a, †], Yoshiyuki Kasai[1], Takaharu Tamaoki[1], Yuki Okabe[1, b], Hideo Fukuhara[1], Jun Kamishikiryo[2], Elena Krayukhina[3, 4], Susumu Uchiyama[3, 4], Toyoyuki Ose[1], Kimiko Kuroki[1] and Katsumi Maenaka[1, ¶]

[1] Laboratory of Biomolecular Science, Faculty of Pharmaceutical Sciences, Hokkaido University, Sapporo, Japan.

[2] Faculty of Pharmacy and Pharmaceutical Sciences, Fukuyama University, Fukuyama, Japan.

[3] Department of Biotechnology, Graduate School of Engineering, Osaka University, , Osaka, Japan.

[4] U-Medico Corporation, Osaka, Japan.

**Key words**: C-type lectin-like receptor, crystal structure, cell surface receptor, Natural killer cell, Protein-protein interactions

[¶]To whom correspondence should be addressed: Katsumi Maenaka, Pharmaceutical Sciences, Hokkaido University, Kita-12, Nishi-6, Kita-ku, Sapporo, Hokkaido, 060-0812,

Japan; Tel: +81-11-706-3970, Fax: +81-11-706-4986; E-mail:

maenaka@pharm.hokudai.ac.jp

**Abbreviations:** AUC, Analytical Ultracentrifugation; CLECs, C-type lectin receptors; Clr, C-type lectin related; CTLD, C-type lectin-like domain; CTLR, C-type lectin-like receptor; LLT1, lectin-like transcript 1; NKRP1, NK receptor-P1; PDB, Protein Data Bank; RMSD, root-mean-square deviation

[†]Equal contribution

Present addresses:

[a]Structural Biology Research Center, Photon Factory, Institute of Materials Structure Science, High Energy Accelerator Research Organization (KEK), Tsukuba, Ibaraki 305-0801, Japan; The Graduate University for Advanced Studies; Department of Materials Structure Science

[b]Research Center for Hepatitis and Immunology, National Center for Global Health and Medicine, 1-7-1 Kohnodai, Ichikawa, Chiba 272-8516, Japan

**ABSTRACT**

Emerging evidence has revealed the pivotal roles of C-type lectin–like receptors (CTLRs) in the regulation of a wide range of immune responses. Human natural killer cell receptor-P1A (NKRP1A) is one of the CTLRs and recognizes another CTLR, lectin-like transcript 1 (LLT1) on target cells to control NK, NKT and Th17 cells. The structural basis for the NKRP1A-LLT1 interaction was limitedly understood. Here, we report the crystal structure of the ectodomain of LLT1. The plausible receptor-binding face of the C-type lectin-like domain (CTLD) is flat, and forms an extended β-sheet. The residues of this face are relatively conserved with another CTLR, keratinocyte-associated C-type lectin (KACL), which binds to the CTLR member, NKp65. A LLT1-NKRP1A complex model, prepared using the crystal structures of LLT1 and the KACL-NKp65 complex, reasonably satisfies the charge consistency and the conformational complementarity to explain a previous mutagenesis study. Furthermore, crystal packing and analytical ultracentrifugation revealed dimer formation, which supports a complex model. Our results provide structural insights for understanding the binding modes and signal transduction mechanisms, which are likely

to be conserved in the CTLR family, and for further rational drug design towards regulating the LLT1 function.

## INTRODUCTION

Natural killer (NK) cells are a component of innate immunity, and display cytotoxic activities against tumor cells and virally infected cells [1, 2]. The activities of NK cells are precisely regulated by activating and inhibitory signals, through diverse receptors on the cell surface [3−5]. These receptors are encoded in two genomic regions, the leukocyte receptor complex (LRC; chromosome 19 in human) [6] and the NK gene complex (NKC; chromosome 12 in human) [7, 8]. The LRC encodes the NK receptors of the immunoglobulin (Ig) superfamily, such as killer Ig-like receptors (KIRs) and leukocyte Ig-like receptors (LILRs), whereas the NKC region encodes the NK receptors of the C-type lectin-like receptors (CTLRs). The CTLRs are subdivided into two groups, according to their expression patterns. Killer cell lectin-like receptors (KLRs) are expressed in NK cells, and C-type lectin receptors (CLECs) are expressed in non-NK cells [9]. The ligands of KLRs are 1) major histocompatibility complex (MHC) class I

molecules and relatives, and 2) CLECs. The former members include CD94, the NKG2 subfamily [10] and the Ly49 subfamily [11], and the latter members are the NK receptor-P1 (NKRP1) subfamily [12, 13].

The NKRP1 subfamily molecules are type II transmembrane glycoproteins, which contain an amino-terminal cytoplasmic domain, a single transmembrane domain followed by a stalk region, and a single extracellular C-type lectin-like domain (CTLD) [13]. Some members of the NKRP1 subfamily contain cysteine residues within the stalk region and form disulfide-linked homodimers [14–16]. The CTLDs are responsible for ligand recognition. Mice have several NKRP1 molecules (Nkrp1a, c, d, f and g), which include both activating and inhibitory receptors. The ligands for the murine NKRP1 family molecules were identified as C-type lectin-related (Clr) molecules (Clr-a, -b, -c, -d, -f, -g and -h). In human, only one NKRP1, NKRP1A (also referred to as CD161, KLRB1 or CLEC5B), has been identified. NKRP1A primarily recognizes the lectin-like transcript 1 (LLT1) expressed on antigen-presenting cells [17−19]. NKRP1A has an immunoreceptor tyrosine-based inhibitory motif (ITIM) in its intracellular region, and functions as an inhibitory receptor. Notably, while NKRP1A is expressed in NK and

NKT cells, NKRP1A is an important marker for Th17 cells, and its expression is induced in a retinoic acid-related orphan receptor C (RORC)-dependent manner. Therefore, the NKRP1A-LLT1 recognition regulates the immune functions of NK, NKT and Th17 cells [20].

In addition to NKRP1A, NKp65 and NKp80 also belong to the human NKRP1 subfamily. The ligands of these molecules are keratinocyte-associated C-type lectin (KACL) and activation-induced C-type lectin (AICL), respectively, and they all belong to the CLEC2 subfamily [21, 22]. The expression patterns and downstream signaling and ligand-receptor interactions of the NKRP1 subfamily receptors and their ligands have been investigated. The binding affinities between the ligands and the receptors were quite diverse. LLT1 and AICL bind their ligands, NKRP1A and NKp80, respectively, with low affinity (LLT1-NKRP1A: Kd ~50 μM [23], AICL-NKp80: Kd ~4 μM [14]), whereas NKp65 binds to KACL with significantly higher affinity (Kd ~0.01 μM) [15]. Since these differences are strongly correlated with the recognition mechanisms, further structural studies at atomic resolution will be required for their clarification.

The structures of NKRP1 members were reported for human CD69, the mouse Clr-G proteins (PDB ID: 3RS1) [24] and mouse Nkrp1a (PDB IDs: 3M9Z and 3T3A) [25, 26]. Their ectodomains adopt the C-type lectin fold, composed of two α-helices and two antiparallel β-sheets [27]. They also form the typical dimer structure seen in the CTLR structures. Recently, the structure of the KACL-NKp65 complex was reported [28]. This was the first structure of a ligand-receptor complex with the CTLD. The binding interfaces of KACL and NKp65 are the membrane-distal sites commonly utilized in CTLRs. The binding topology involved the KACL dimer binding to two NKp65 monomers. The KACL-NKp65 complex structure has facilitated an understanding of the structurally related LLT1-NKRP1A recognition, although the binding affinity and disulfide formation relevant for functional signaling are distinct between these two systems. To understand the signaling by LLT1-NKRP1A in comparison with those by other CTLRs, we have investigated the molecular mechanism of LLT1 recognition by NKRP1A. We previously revealed the biophysical characteristics of the LLT1-NKRP1A interaction, including the kinetic and thermodynamic properties, by a surface plasmon resonance analysis [23]. Based on a broad mutagenesis study, we identified the binding

sites for both LLT1 and NKRP1A as the membrane distal areas, which are also utilized for ligand binding by other CTLRs (e.g. CD94-NKG2-MHCI [29, 30] and KLRG1-E-cadherin [31]). We further proposed a rough binding topology template for the ligand interactions of NKRP1s. However, the structures of LLT1 and NKRP1A were not available. Here we report the first crystal structure of the LLT1 ectodomain, which is responsible for receptor recognition. The putative receptor binding face exhibits structural characteristics that are relatively conserved with those of KACL. We constructed a model of the LLT1-NKRP1A complex that reasonably explains the receptor binding and specificity, by electrostatic, hydrophobic, and shape complementarity interactions. We discuss the similarities and differences of the LLT1-NKRP1A signaling system from those of other CTLRs, including Clr-Nkrp1, KACL-NKp65 and AICL-NKp80.

## RESULTS

*Sample preparation, crystallization and structure determination of LLT1*

The LLT1 H176C mutant protein, hereafter simply designated as LLT1 was expressed in *E. coli* as inclusion bodies and refolded by the dilution method, as reported previously [23]. After the refolding, the protein was concentrated and purified by size exclusion chromatography (SEC), as a monomer, where majority of the LLT1 was apparently eluted at 18kDa, slightly larger than monomer value (14kDa) calculated from the amino acid sequence (**Fig. 1A**). The homogeneity of the purified protein was determined to be >90% by SDS-PAGE. In the initial crystallization screening, crystals of LLT1 were obtained using commercial kits, PACT Suite (QIAGEN) and Wizard I & II (Emerald BioSystems). However, the crystals were small and the resolution was poor (up to 7 Å). Despite further screening of the crystallization conditions, no crystals providing good diffraction were obtained. Hence, the seeding method was applied to generate single larger crystals, and finally, crystals that diffracted to 2.46 Å resolution were obtained (**Fig. 1B**). The X-ray diffraction dataset was collected on the beamline NW12A of the Photon Factory (Tsukuba, Japan). Using the diffraction data, the LLT1

structure was solved by the molecular replacement method, with the crystal structure of CD69 (PDB ID: 3HUP) [32] as a search model. The model of LLT1 was refined until the value of $R$ and $R_{free}$ factors converged using refinement programs. In the refined model, electron density maps of side chains are clearly observed (**Fig. 1C**).

*Overall structure of LLT1*

In the asymmetric unit, three molecules (A, B and C) were observed. The molecules superimposed well on each other, with Cα r.m.s.d. values of 0.57 Å (A-B), 0.55 Å (A-C) and 0.39 Å (B-C) (**Supporting Information Fig. 1A**). Hereafter, we will focus on the structural features of LLT1 based on molecule A, as a representative structure. LLT1 adopts the typical C-type lectin-like fold composed of two α-helices (α1 and α2) and two anti-parallel β-sheets (β0-β1-β5-β1' and β2'-β2-β3-β4-β2") (**Fig. 1D and 1F**). The two β-sheets are located at the center of the molecule, and are nearly perpendicular to each other. The core β-strands (β1-β5-β1' and β2-β3-β4) are common in the CTLD superfamily members [27]. A structural similarity search using the DALI server [33] identified the CLECs with high Z-scores. From the top, they are Clr-G (PDB ID: 3RS1,

Z-score: 21.7), CD69 (PDB ID: 1E8I, Z-score: 21.1) and KACL (PDB ID: 4IOP, Z-score: 20.5). Accordingly, the monomer structure of LLT1 superimposes well onto these CLECs (Superimpositions of LLT1 onto Clr-G, CD69 and KACL yielded Cα r.m.s.d. values of 0.83 Å, 0.88 Å, and 0.93 Å, respectively.) (**Supporting Information Fig. 1B**), except for the region corresponding to the β-strands, β2' and β2", with non-structured loop connections (residues 137-162) of LLT1. Although the region of LLT1 exhibits the compact fold fixed by the β2' and β2" strands, the corresponding regions of some C-type lectin-like proteins are flipped toward the outside of the molecules, and thus lack these β-strands (e.g. Nkrp1a and Flavocetin, (**Fig. 1D and 1E**))[25, 26, 34]. The *B*-factors of the loop connections are relatively high as compared with the rest of the structure, but those corresponding to these β strands are not very high, indicating that the two β-sheets are stable in the LLT1 structure (**Supporting Information Fig. 2**). Three disulfide bonds (Cys75-Cys86, Cys103-Cys184 and Cys163-Cys176) are present in the structure (**Fig. 1D and Supporting Informaiton Fig. 1C**). Our previous study revealed that the wild-type LLT1 harboring His176 is not stable and easily aggregated, but the LLT1 H176C mutant is much more stable and

soluble [23], and could be crystallized as described above. In the wild-type LLT1, the free Cys163 likely contributes to facilitate aggregation, possibly due to additional disulfide bond formation and/or exposure of hydrophobic region to outside, which would not occur on the cell surface. The present structure shows that Cys176 forms a disulfide bond with Cys163, which is often observed at the corresponding sites of CTLR members, thus improving the stability of the LLT1 proteins.

In the crystal structure, zinc ions, which are components of the crystallization buffer, were found between the LLT1 molecules and identified from the anomalous differential fourier map, suggesting that they facilitate the molecular packing of the LLT1 crystals (**Supporting Information Fig. 3A**). There are four putative calcium-binding sites in the CTLD superfamily [27]. The observed zinc-binding sites in LLT1 are different from these calcium-binding sites (**Supporting Information Fig. 3B and 3C**). The calcium-binding motifs are not conserved in the LLT1 sequence, and no residual maps were observed around the potential calcium-binding sites, indicating that the observed zinc molecules are merely derived from the crystallization buffer, and are not substitutes for the calcium ions.

*Characteristics of the putative receptor binding face of LLT1*

The membrane distal part of LLT1 forms a flat 24 Å-square face (**Fig. 2A and 2B**). This face is a typical ligand-receptor recognition site in the CTLRs, such as KACL, NKp65, NKG2D and KLRG1, which all share proteinaceous binding partners. The face in LLT1 includes charged residues, such as the positively charged Lys169, Arg175 and Lys181, and the negatively charged Asp168 and Glu179. All of these residues are located on the edge of the plane and protrude outward from the flat surface. At the center, Arg180 interacts with Asp130, and also makes a typical π-cation interaction with Tyr165 and Trp132 (**Fig. 1C**), which results in the formation of a small hydrophobic patch with Ala174. Hydrophobic residues, Leu158 and Tyr177, also exist at the edge of the face. The previous mutagenesis study clearly revealed that the mutations of the positively-charged residues mentioned here (Lys169, Arg175, Arg180 and Lys181) with glutamic acids caused detrimental effects on the binding, suggesting that the charge distribution is critical for the recognition. The surface potentials on the corresponding faces of other CTLRs are depicted in **Supporting Information Fig. 4**. The surfaces in

LLT1 and Clr-G are predominantly positively charged. The positively charged patch of LLT1 is mainly composed of Lys169, Arg175 and Arg180, as well as several exposed main-chain amide groups (Ala171, Ser172, Ser173 and Ala174). Negatively charged residues also exist, as described above. The structure of the KACL-NKp65 complex, which was the only one reported for the ligand complex structure of CTLRs, the positive patch of KACL binds the negative patch of NKp65 and vice versa. NKRP1A is also expected to have an electrostatically complementary surface with that of LLT1 (**Supporting Information Fig. 4**).

*LLT1 homodimers*

Among the three molecules in the asymmetric unit, molecules A and B form a dimer related by a non-crystallographic two-fold axis. In the dimer, the N-terminal ends are oriented toward the center of the dimer and form the butterfly-like structure generally seen in CTLRs (**Fig. 2C**). Molecule C also forms a dimer related by a crystallographic two-fold axis. These homodimers (A-B and C-C) are essentially similar (Cα r.m.s.d. of 1.00 Å). We then performed the sedimentation velocity analytical ultracentrifugation to

investigate the oligomeric state of the LLT1 in solution. The result clearly showed that the LLT1 exists in dimer with minor fraction of monomer in the solution (**Fig. 2D**), leading to the conclusion that the dimer structure in the crystal is not the artifact of the crystal packing, but it certainly reflects the assembly state in the solution. Superimposition of the LLT1 homodimer (A-B, as a representative dimer) onto KACL, Clr-G and CD69 generated Cα r.m.s.d. values of 1.70, 1.58 and 2.29 Å, respectively, suggesting that the dimer structures of LLT1 are conserved with those of other CTLRs (**Fig. 2C**). The dimer is mainly formed by the hydrophobic interactions in the center of the dimer interface and the hydrogen bond network between α2 and β0, surrounding the hydrophobic core. Between the α2s, the amide groups of the Arg124 side chain contact the carbonyl oxygen of Lys126 (**Supporting Information Fig. 5**). Additionally, in the C-C homodimer, an anti-parallel β-sheet is formed between the β0s. On the other hand, between the β0s in the A-B homodimer, the carbonyl oxygen of Trp79 contacts the amide group of Gln72, and the carbonyl oxygen of Cys75 contacts the carbonyl oxygen of Gln72. The amino acid residues involved in hydrophobic interactions and hydrogen bonds are conserved among the other CLEC2s (**Fig. 1E**). Hence, the dimer formation

mechanism is basically conserved among CLEC2s. On the cell surface, LLT1 is known to form a homodimer via disulfide bond(s) in the N-terminal stalk region, which is missing in the present study. Thus, the dimer structures of LLT1 seen in the crystals are likely to reflect the structures on the cell surface.

## DISCUSSION

We have determined the crystal structure of LLT1, which revealed the structural features and assembly state. The DALI server search showed that LLT1 shares structural similarity with Clr-G, CD69, KACL, CLEC5A and KLRG1, which all belong to the type V group (NK cell receptors) in the CTLD superfamily [27]. We previously constructed the binding model of the LLT1-NKRP1A complex, based on the interaction analysis by SPR. The structures of both LLT1 and NKRP1A were built using the homology modeling server, Swiss-Model [35], since the structures of LLT1 and NKRP1A were not available at that time. To discuss the binding topology of LLT and NKRP1A, the residues involved in the KACL binding to Nkp65 were structurally compared with those on the putative receptor binding face of LLT1 (**Fig. 3**) [28]. The characteristically conserved receptor-binding residues are Thr93/Thr, Leu158/Ile, Tyr165/Phe, Ser173/Ser, Arg175/Arg, Tyr177/Phe and Glu179/Asp (LLT1/KACL). On the other hand, the non-conserved residues are located in adjacent two patches consisting of 1) Pro128/Thr, Ser129/Asp and Asp130/Met, and 2) Lys169/Asp and Ser172/His (LLT1/KACL). They are likely to be involved in the determination of the

binding specificity. Sequence alignment between NKRP1A and NK65p shows that most of the residues on NKp65 ligand binding face involved with KACL-NKp65 recognition are characteristically conserved (**Fig. 3C)**. It suggests that the binding topology of LLT1-NKRP1A is similar with that of KACL-NKp65. Furthermore, the unliganded LLT1 structure is essentially similar to KACL in complex with NKp65, raising the possibility that KACL and LLT1 do not show any significant induced fit on the complex formation. Hence, by reference to the structure of KACL-NKp65 complex, we constructed a new binding model. We superimposed structures of LLT1 and mouse Nkrp1a (either the solution structure or the crystal structure) onto the KACL-NKp65 complex structure. Using this binding model, the positions of the key residues, confirmed by the previous SPR analysis [23], and their putative interaction partners are shown in **Supporting Information Fig. 6**. The hydrophobic residues on the surface of LLT1, Tyr165 and Tyr177, are located near the positions of Phe152 (with Leu151 and Ile206) and Tyr198 in NKRP1A, respectively. The basic residues in LLT1, Lys169 and Arg175, likely make contacts with Glu205 and Glu200 in NKRP1A, respectively. The acidic residue, Glu179 in LLT1, is located near Ser193 (with Thr195) in NKRP1A.

Accordingly, the LLT1-NKRP1A model reasonably explains the binding mode. Especially, the mutagenesis study identified Lys169 (LLT1) and Glu205 (NKRP1A) as binding partners, which were confirmed in the model. Although a slight rotation and/or transformation may be required to reflect the true complex structure, the updated LLT1-NKRP1A model sufficiently represents the binding mode for understanding LLT1-NKRP1A signaling.

Next, we further considered the bivalent mode, since both LLT1 and NKRP1A are believed to form disulfide-bonded homodimers on the cell surface [14–16]. Furthermore, the present analytical ultracentrifugation clearly showed the dominant existence of the dimers of LLT1. Therefore, the bivalent binding model was constructed, based on the dimer structure of LLT1 (dimer A-B) observed in the asymmetric unit (**Fig. 2C)**. In the bivalent model, NKRP1A showed no severe steric hindrance between the monomers. This strongly supports the validity of the present model. The residues with less detrimental effects when mutated, such as Glu179, Arg181, Asp183, Lys185 and Glu186 in NKRP1A, are outside of the interface and located in the region between the β2 and β3 strands, which adopts significantly different conformations of the canonical

C-type lectin-like domains. In the crystal structure of Nkrp1a (PDB ID: 3M9Z), the corresponding region is flipped out from the molecule and forms tight contacts with the neighboring Nkrp1a molecule in the crystals. Similarly, the CTLRs harboring the extended long loop form homodimers via the intermolecular interactions of these loops [25, 26, 36]. On the other hand, this extended loop is not observed in the solution structure of Nkrp1a solved by NMR analysis (PDB ID: 2M94). Instead, this region exhibits a wing-like structure and forms additional short β-strands, β2' and β2", as in LLT1. In the structure of the KACL-NKp65 complex, the corresponding region of NKp65 similarly folds into a wing-like structure [28]. Taken together, these results support the idea that the regions may change their conformations according to their binding partners. On the cell surface, NKRP1A may form homodimers via the extended loop in the *cis* interaction. However, upon binding to LLT1 on the counter cells, it forms heterodimers in *trans* by adopting the compact conformations of the long loop region. Since the sufficient signaling for the LLT1-NKR-P1A system would further require the multimerization on the cell surface as low-affinity cell-cell recognition receptors, further analyses are required to understand the functional role of the extended loop (**Fig.**

**4**).

To elucidate the specific LLT1-NKRP1A recognition elements that are relevant for the rational design of small molecules and biologics regulating this signaling pathway, an investigation of the differences in the binding recognition with the KACL-NKp65 system is important. The Pro128, Ser129 and Asp130 residues, which differ from those (Thr, Asp and Met, respectively) of KACL, are concentrated in a patch (**Fig. 3 and Supporting Information Fig. 7**). Tyr165, which lies next to this patch in LLT1, corresponds to Phe in KACL, indicating the conservation from the viewpoint of the hydrophobic aromatic part, but the difference in the existence of the hydroxyl group. Ala174, neighboring Tyr165 in LLT1, is changed to Ser in KACL. These substitutions between LLT1 and KACL would differentiate the hydrophobicity of this continuous region. Therefore, the inclusion of this region in the target site of LLT1, for the rational design of small molecule regulators and biologics, would probably enhance the specificity.

In conclusion, the present model of the LLT1-NKRP1A complex, based on the crystal structure of LLT1, provides a potential recognition mode satisfying the charge

consistency and the conformational complementarity conserved among the NKRP1 subfamily members. The model also provides insights into the slight but distinct characteristics relevant for ligand-receptor specificity and rational drug design.

## Materials and Methods

*Expression and purification of LLT1 proteins*

The expression and purification of the LLT1 H176C mutant protein (amino acid residues Leu71-Val191) were performed as described previously [37]. The expression plasmid LLT1/pET22 was transformed into the *Escherichia coli* strain BL21 (DE3) pLysS. The cells were cultured in LB medium with 100 mg/liter ampicillin (Nacalai Tesque, Kyoto, Japan) at 310K. When the A600 reached 0.6, isopropyl β-D-thiogalactopyranoside (Nacalai Tesque) was added for induction, at a final concentration of 1 mM. The recombinant LLT1 protein was expressed as insoluble inclusion bodies. After 4 h of induction, the cells were harvested by centrifugation. The inclusion bodies were isolated from the cell pellet by sonication, and were washed repeatedly with Triton wash buffer (50 mM Tris-HCl, pH 8.0, 100 mM NaCl, 0.5%

Triton X-100). The purified LLT1 inclusion bodies were solubilized in denaturant buffer (50 mM Tris-HCl, pH 8.0, 10 mM EDTA, 6 M guanidine HCl). The solubilized protein solution was slowly diluted by the addition of ice-cold refolding buffer (100 mM Tris-HCl, pH 8.0, 2 mM EDTA, 1 M L-arginine, 3.73 mM cystamine, 6.37 mM cysteamine), to a final protein concentration of 2 mM. After an incubation for 72 h at 277 K, the refolded protein solution was concentrated with a VIVAFLOW50 system (Sartorius). The LLT1 protein was purified by size exclusion chromatography (SEC), using a Superdex 75 column (GE Healthcare) followed by anion exchange chromatography, using a Resource Q column (GE Healthcare). Finally, the protein solution was buffer-exchanged by dialysis against 20 mM MES-NaOH, pH 6.5.

*Sedimentation Velocity Analytical Ultracentrifugation (SV-AUC)*

SV-AUC experiment was performed in 20 mM Tris-HCl (pH 8.5), 50 mM NaCl, using ProteomeLab XL-I Analytical Ultracentrifuge equipped with a 4-hole An60 Ti rotor (Beckman Coulter). Data were collected using an absorbance optical system at a wavelength of 303 nm at 55,000 rpm and at 20°C using Beckman Coulter aluminum

centerpiece. Data were analyzed using the continuous c(*s*) distribution model implemented in the program SEDFIT (version 14.4d) [38]. The partial specific volume of the LLT1 protein, buffer viscosity and buffer density were calculated using the program SEDNTERP 1.09 and were 0.7182 $cm^3/g$, 1.013 cP and 1.0009 g/mL, respectively.

*Crystallization of LLT1*

The purified LLT1, in 20 mM MES-NaOH, pH 6.5, was concentrated to 32 mg/mL, using an Amicon Ultra 5K filter (Millipore), and subsequently used for crystallization. Initial screening was performed with commercially available kits from Emerald BioSystems (Washington, USA) and Qiagen (Hilden, Germany) by the sitting-drop vapor-diffusion method, using a mosquito robot. Briefly, 100 nL of the protein solution was mixed with an equal volume of reservoir solution. Initial crystals of LLT1 were obtained with a reservoir solution containing 0.1 M sodium MES-NaOH, pH 6.0, 0.2 M zinc acetate and 10% (w/v) PEG8000. After the refinement of the crystallization conditions, sufficiently diffracting crystals were obtained in a buffer containing 0.1 M

sodium cacodylate, pH 6.5, 0.2 M zinc acetate and 5% (w/v) PEG8000. For data collection, the crystals of LLT1 were soaked into a cryoprotectant solution containing 18% (v/v) glycerol, and then flash-cooled in a stream of liquid nitrogen at 100K. X-ray diffraction data for LLT1 were collected on the beamline NW12A of the Photon Factory (Tsukuba, Japan).

*Structure determination of LLT1*

The data set for LLT1 was processed using the *HKL-2000* program suite [39]. The structure was determined by the molecular replacement (MR) method with the program *BALBES* in the *CCP4* suite [40], using the structure of CD69 (PDB ID: 3HUP) [32] as a search model. Rotation and translation functions were calculated using data from 50.0 to 3.5 Å resolution. The structures were modified manually with *Coot* [41] and refined with *Refmac5* [42] and *phenix.refine* [43]. To clarify the residual-density map in the structure, another dataset was collected at the peak of zinc anomalous signals (1.28 Å). The final model was assessed to have good stereochemical quality by the program *Molprobity* [44]. The data collection and refinement statistics are summarized in Table

1. Coordinates and structure factors were deposited in the RCSB Protein Data Bank (http://www.rcsb.org/pdb/home/home.do), under the accession code (PDB ID: 4 WCO). The structural similarity search was performed using the DALI server [33]. Structures were displayed using PyMOL (PyMOL Molecular Graphics System).

**ACKNOWLEDGEMENTS**

We thank the beamline staff of the Photon Factory and SPring-8 for their assistance with X-ray diffraction data collection. We also thank Dr. T. Tadokoro for helpful discussion. This work was supported in part by Platform for Drug Discovery, Informatics, and Structural Life Science and other grants from the Ministry of Education, Culture, Sports, Science and Technology and the Ministry of Health, Labor and Welfare of Japan.

**Conflict of Interest Disclosure**

The authors declare no commercial or financial conflict of interest.

**REFERENCES**


1. **Vivier E, Tomasello E, Baratin M, Walzer T, Ugolini S**. Functions of natural killer cells. *Nat. Immunol.* 2008; **9**:503–10.DOI: 10.1038/ni1582.

2. **Di Santo JP**. Natural killer cells: diversity in search of a niche. *Nat. Immunol.* 2008; **9**:473–5.DOI: 10.1038/ni.f.201.

3. **Bryceson YT, Chiang SCC, Darmanin S, Fauriat C, Schlums H, Theorell J, Wood SM**. Molecular mechanisms of natural killer cell activation. *J. Innate Immun.* 2011; **3**:216–26.DOI: 10.1159/000325265.

4. **Kuroki K, Furukawa A, Maenaka K**. Molecular recognition of paired receptors in the immune system. *Front. Microbiol.* 2012; **3**:429.DOI: 10.3389/fmicb.2012.00429.

5. **Cooper M**. NK cell and DC interactions. *Trends Immunol.* 2004; **25**:47–52.DOI: 10.1016/j.it.2003.10.012.

6. **Barrow AD, Trowsdale J**. The extended human leukocyte receptor complex: diverse ways of modulating immune responses. *Immunol. Rev.* 2008; **224**:98–123.DOI: 10.1111/j.1600-065X.2008.00653.x.

7. **Yokoyama WM, Plougastel BFM**. Immune functions encoded by the natural killer gene complex. *Nat. Rev. Immunol.* 2003; **3**:304–16.DOI: 10.1038/nri1055.

8. **Kelley J, Walter L, Trowsdale J**. Comparative genomics of natural killer cell receptor gene clusters. *PLoS Genet.* 2005; **1**:129–39.DOI: 10.1371/journal.pgen.0010027.

9. **Bartel Y, Bauer B, Steinle A**. Modulation of NK cell function by genetically coupled C-type lectin-like receptor/ligand pairs encoded in the human natural killer gene complex. *Front. Immunol.* 2013; **4**:362.DOI: 10.3389/fimmu.2013.00362.

10. **Borrego F, Marusina AI, Coligan JE**. The CD94 / NKG2 Family of Receptors. 2006:263–277.

11. **Rahim MM a, Tu MM, Mahmoud AB, Wight A, Abou-Samra E, Lima PD a, Makrigiannis AP**. Ly49 receptors: innate and adaptive immune paradigms. *Front. Immunol.* 2014; **5**:145.DOI: 10.3389/fimmu.2014.00145.

12. **Kirkham CL, Carlyle JR**. Complexity and Diversity of the NKR-P1:Clr (Klrb1:Clec2) Recognition Systems. *Front. Immunol.* 2014; **5**:214.DOI: 10.3389/fimmu.2014.00214.

13. **Ljutic B, Makrigiannis AP, Carlyle JR**. NKR-P1 Biology. 2006:13–26.

14. **Welte S, Kuttruff S, Waldhauer I, Steinle A**. Mutual activation of natural killer cells and monocytes mediated by NKp80-AICL interaction. *Nat. Immunol.* 2006; **7**:1334–42.DOI: 10.1038/ni1402.

15. **Spreu J, Kuttruff S, Stejfova V, Dennehy KM, Schittek B, Steinle A**. Interaction of C-type lectin-like receptors NKp65 and KACL facilitates dedicated immune recognition of human keratinocytes. *Proc. Natl. Acad. Sci. U. S. A.* 2010; **107**:5100–5.DOI: 10.1073/pnas.0913108107.

16. **Mathew P**. The LLT1 receptor induces IFN-γ production by human natural killer cells. *Mol. Immunol.* 2004; **40**:1157–1163.DOI: 10.1016/j.molimm.2003.11.024.

17. **Rosen DB, Cao W, Avery DT, Stuart G, Liu Y, Houchins JP, Lanier LL, *et al.*** NKR-P1A and Its Ligand LLT1 Expressed on Activated. 2013.

18. **Satkunanathan S, Kumar N, Bajorek M, Purbhoo M a, Culley FJ**. Respiratory syncytial virus infection, TLR3 ligands, and proinflammatory cytokines induce CD161 ligand LLT1 expression on the respiratory epithelium. *J. Virol.* 2014; **88**:2366–73.DOI: 10.1128/JVI.02789-13.

19. **Cells D, Cells B, Rosen DB, Cao W, Avery DT, Tangye SG, Liu Y, *et al.*** Functional Consequences of Interactions between Human NKR-P1A and Its Ligand LLT1 Expressed on Activated. 2008.

20. **Germain C, Meier A, Jensen T, Knapnougel P, Poupon G, Lazzari A, Neisig A, *et al.*** Induction of lectin-like transcript 1 (LLT1) protein cell surface expression by pathogens and interferon-γ contributes to modulate immune responses. *J. Biol. Chem.* 2011; **286**:37964–75.DOI: 10.1074/jbc.M111.285312.

21. **Vogler I, Steinle A**. Vis-à-vis in the NKC: genetically linked natural killer cell receptor/ligand pairs in the natural killer gene complex (NKC). *J. Innate Immun.* 2011; **3**:227–35.DOI: 10.1159/000324112.

22. **Aldemir H, Prod'homme V, Dumaurier M-J, Retiere C, Poupon G, Cazareth J, Bihl F, *et al.*** Cutting edge: lectin-like transcript 1 is a ligand for the CD161 receptor. *J. Immunol.* 2005; **175**:7791–5.

23. **Kamishikiryo J, Fukuhara H, Okabe Y, Kuroki K, Maenaka K**. Molecular basis for LLT1 protein recognition by human CD161 protein (NKRP1A/KLRB1). *J. Biol. Chem.* 2011; **286**:23823–30.DOI: 10.1074/jbc.M110.214254.

24. **Skálová T, Kotýnková K, Dusková J, Hasek J, Kova T, Kolenko P, Novák P, *et al.*** Mouse Clr-g, a Ligand for NK Cell Activation Receptor NKR-P1F: Crystal Structure and Biophysical Properties. 2013.DOI: 10.4049/jimmunol.1200880.

25. **Kolenko P, Rozbeský D, Vaněk O, Kopecký V, Hofbauerová K, Novák P, Pompach P, *et al.*** Molecular architecture of mouse activating NKR-P1 receptors. *J. Struct. Biol.* 2011; **175**:434–41.DOI: 10.1016/j.jsb.2011.05.001.

26. **Kolenko P, Rozbeský D, Vaněk O, Bezouška K, Hašek J, Dohnálek J**. Structure of the H107R variant of the extracellular domain of mouse NKR-P1A at 2.3 Å resolution. *Acta Crystallogr. Sect. F. Struct. Biol. Cryst. Commun.* 2011; **67**:1519–23.DOI: 10.1107/S1744309111046203.

27. **Zelensky AN, Gready JE**. The C-type lectin-like domain superfamily. *FEBS J.* 2005; **272**:6179–217.DOI: 10.1111/j.1742-4658.2005.05031.x.

28. **Li Y, Wang Q, Chen S, Brown PH, Mariuzza R a**. Structure of NKp65 bound to its keratinocyte ligand reveals basis for genetically linked recognition in natural killer

gene complex. *Proc. Natl. Acad. Sci. U. S. A.* 2013; **110**:11505–10.DOI: 10.1073/pnas.1303300110.

29. **Petrie EJ, Clements CS, Lin J, Sullivan LC, Johnson D, Huyton T, Heroux A, *et al.*** CD94-NKG2A recognition of human leukocyte antigen (HLA)-E bound to an HLA class I leader sequence. *J. Exp. Med.* 2008; **205**:725–35.DOI: 10.1084/jem.20072525.

30. **Kaiser BK, Pizarro JC, Kerns J, Strong RK**. Structural basis for NKG2A/CD94 recognition of HLA-E. *Proc. Natl. Acad. Sci. U. S. A.* 2008; **105**:6696–701.DOI: 10.1073/pnas.0802736105.

31. **Li Y, Hofmann M, Wang Q, Teng L, Chlewicki LK, Pircher H, Mariuzza RA**. Article Structure of Natural Killer Cell Receptor KLRG1 Bound to E-Cadherin Reveals Basis for MHC-Independent Missing Self Recognition. *Immunity*. 2009; **31**:35–46.DOI: 10.1016/j.immuni.2009.04.019.

32. **Kolenko P, Skálová T, Vanek O, Stepánková A, Dusková J, Hasek J, Bezouska K, *et al.*** The high-resolution structure of the extracellular domain of human CD69 using a novel polymer. *Acta Crystallogr. Sect. F. Struct. Biol. Cryst. Commun.* 2009; **65**:1258–60.DOI: 10.1107/S1744309109043152.

33. **Holm L, Rosenström P**. Dali server: conservation mapping in 3D. *Nucleic Acids Res.* 2010; **38**:W545–9.DOI: 10.1093/nar/gkq366.

34. **Fukuda K, Mizuno H, Atoda H, Morita T**. Crystal Structure of Flavocetin-A , a Platelet Glycoprotein Ib-Binding Protein , Reveals a Novel Cyclic Tetramer of C-Type Lectin-like Heterodimers †,‡. 2000:1915–1923.

35. **Guex N, Peitsch MC, Schwede T**. Automated comparative protein structure modeling with SWISS-MODEL and Swiss-PdbViewer: a historical perspective. *Electrophoresis*. 2009; **30 Suppl 1**:S162–73.DOI: 10.1002/elps.200900140.

36. **Sovová Z, Kopecký V, Pazderka T, Hofbauerová K, Rozbeský D, Vaněk O, Bezouška K, *et al.*** Structural analysis of natural killer cell receptor protein 1 (NKR-P1)

extracellular domains suggests a conserved long loop region involved in ligand specificity. *J. Mol. Model.* 2011; **17**:1353–70.DOI: 10.1007/s00894-010-0837-y.

37. **Kamishikiryo J, Fukuhara H, Okabe Y, Kuroki K, Maenaka K**. Molecular basis for LLT1 protein recognition by human CD161 protein (NKRP1A/KLRB1). *J. Biol. Chem.* 2011; **286**:23823–23830.DOI: 10.1074/jbc.M110.214254.

38. **Schuck P**. Size-Distribution Analysis of Macromolecules by Sedimentation Velocity Ultracentrifugation and Lamm Equation Modeling. 2000; **78**:1606–1619.

39. **Kaplan NO, Colowick SP, Abelson JN, Simon MI, Carter CW, Sweet RM**. *Methods in Enzymology: Macromolecular crystallography: Part A, Volume 276*. Academic Press; 1997:700.

40. **Long F, Vagin A a, Young P, Murshudov GN**. BALBES: a molecular-replacement pipeline. *Acta Crystallogr. D. Biol. Crystallogr.* 2008; **64**:125–32.DOI: 10.1107/S0907444907050172.

41. **Emsley P, Lohkamp B, Scott WG, Cowtan K**. Features and development of Coot. *Acta Crystallogr. D. Biol. Crystallogr.* 2010; **66**:486–501.DOI: 10.1107/S0907444910007493.

42. **Murshudov GN, Skubák P, Lebedev A a, Pannu NS, Steiner R a, Nicholls R a, Winn MD, *et al.*** REFMAC5 for the refinement of macromolecular crystal structures. *Acta Crystallogr. D. Biol. Crystallogr.* 2011; **67**:355–67.DOI: 10.1107/S0907444911001314.

43. **Adams PD, Afonine P V, Bunkóczi G, Chen VB, Davis IW, Echols N, Headd JJ, *et al.*** PHENIX: a comprehensive Python-based system for macromolecular structure solution. *Acta Crystallogr. D. Biol. Crystallogr.* 2010; **66**:213–21.DOI: 10.1107/S0907444909052925.

44. **Chen VB, Arendall WB, Headd JJ, Keedy DA, Immormino RM, Kapral GJ, Murray LW, *et al.*** MolProbity: all-atom structure validation for macromolecular

crystallography. *Acta Crystallogr. D. Biol. Crystallogr.* 2010; **66**:12–21.DOI: 10.1107/S0907444909042073.

45. **Bond CS, Schüttelkopf AW**. ALINE: a WYSIWYG protein-sequence alignment editor for publication-quality alignments. *Acta Crystallogr. D. Biol. Crystallogr.* 2009; **65**:510–2.DOI: 10.1107/S0907444909007835.

## FIGURE LEGENDS

**FIGURE 1. Preparation and crystal structure of LLT1.**

*A.* Chromatogram of SEC. The sizes of the standard proteins are shown at their elution positions. The purity of the sample was confirmed by SDS-PAGE. *B.* Pictures of the obtained LLT1 crystals. The black bar indicates 100 μm. *C.* The electron densities of the Trp132, Tyr165 and Arg180 residues, shown in stereoview. The 2*F*o-*F*c map of LLT1 is contoured at 1σ. *D.* The overall structure of LLT1, displayed as a ribbon diagram. The structure of LLT1 is composed of two α-helices and two β-sheets. The α-helices and β-strands are colored green and purple, respectively. The β-strands, β2' and β2", with non-structured loop connections (residues 137-162), are colored cyan. Intramolecular disulfide bonds (Cys75-Cys86, Cys103-Cys184 and Cys163-Cys176) are shown in yellow. The stalk region connecting CTLD with membrane is shown as dotted line with two cysteine residues. The N-terminal and C-terminal ends are shown as N and C, respectively. *E.* Structures of KACL (PDB ID: 4IOP), Nkrp1a (PDB ID: 3M9Z) and Flavocetin (PDB ID: 1C3A), with the same orientation and colors as in D. The region corresponding to the long loop region connecting β2 and β3 (including β2'and β2"

strands) in LLT1 is flipped out in Nkrp1a and Flavocetin and are marked as dotted lines. *F*. Sequence alignment of different CLECs. The secondary structure elements of LLT1 are shown above the sequences. The position of the H176C mutation is denoted by an asterisk. The β-strands, β2' and β2", with non-structured loop connections (residues 137-162) are indicated by the dotted line in cyan. The residues located at the interface of LLT1 homodimer is denoted as dimer with line above the sequence. This figure was drawn with ALINE [45].

**FIGURE 2. Putative receptor binding face and dimer formation of LLT1.**

*A and B*. The structure of LLT1, shown in the same orientation as in Figure 1D (A), and the $90^{o}$ rotated structure (B). The residues oriented outward are represented by sticks. The positively charged residues, Lys169, Arg175 and Lys181, are colored dark blue, and the negatively charged residues, Asp168 and Glu179, are colored red. The residues forming the hydrophobic patch (residues Asp130, Tyr165, Ala174 and Arg180) at the center of the face are colored magenta. The hydrophobic residues, Tyr177 and Leu158, located at the edge of the face, are colored orange. The residues whose main chain

amide groups (Ala171, Ser172, Ser173 and Ala174) contribute to the positively charged patch are shown as stick (main chain C, N and O atoms are colored in gray, blue and red, respectively). *C.* The structure of the LLT1 homodimer (A-B, dark blue) is compared with those of the LLT1 homodimer (C-C, purple (top)) and the KACL homodimer (orange (bottom)). Superimpositions of the LLT1 homodimer (A-B) onto the LLT1 homodimer (C-C) and KACL generated Cα r.m.s.d. values of 1.00 and 1.70 Å, respectively. *D.* Analytical ultracentrifugation experiments. Plot of the distribution of sedimentation coefficients (s versus *C*(s), where s is plotted in Sverdberg units, S) calculated from SV-AUC experiments. One representative plot out of two experiments is shown.

**FIGURE 3. Ligand-receptor binding interfaces of the LLT1-NKRP1A and KACL-NKp65 complexes.**

*A and B.* The ligand-receptor binding interfaces of (A) LLT1 and NKRP1A and (B) KACL and NKp65 shown in same orientation as Fig. 3 right panel. The residues involved in the KACL-NKp65 interaction are represented as sticks. These residues are

categorized into six groups and drawn in different colors (red, orange, cyan, green, blue and magenta) according to their location in the KACL-NKp65 complex. The residues of LLT1 occupying same positions as corresponding residues of KACL are drawn in same colors. The residues, which may be involved in LLT1-NKRP1A interaction, are predicted from the sequence alignment of NKRP1A and NKp65. According to these residues, the surface of NKRP1A is divided into 6 groups and drawn in same color as NKp65. *C.* Sequence alignment of the receptor binding faces of LLT1-KACL (top) and NKRP1A-NKp65 (bottom). The residues shown in *A and B* are drawn as same color.

**FIGURE 4. LLT1-NKRP1A binding topology on the cell surface.**

LLT1-NKRP1A binding model in the bivalent mode is displayed as ribbon representation. LLT1 and NKRP1A are colored as dark blue and green, respectively. The orientation of the LLT1 homodimer is same as Figure 2C.

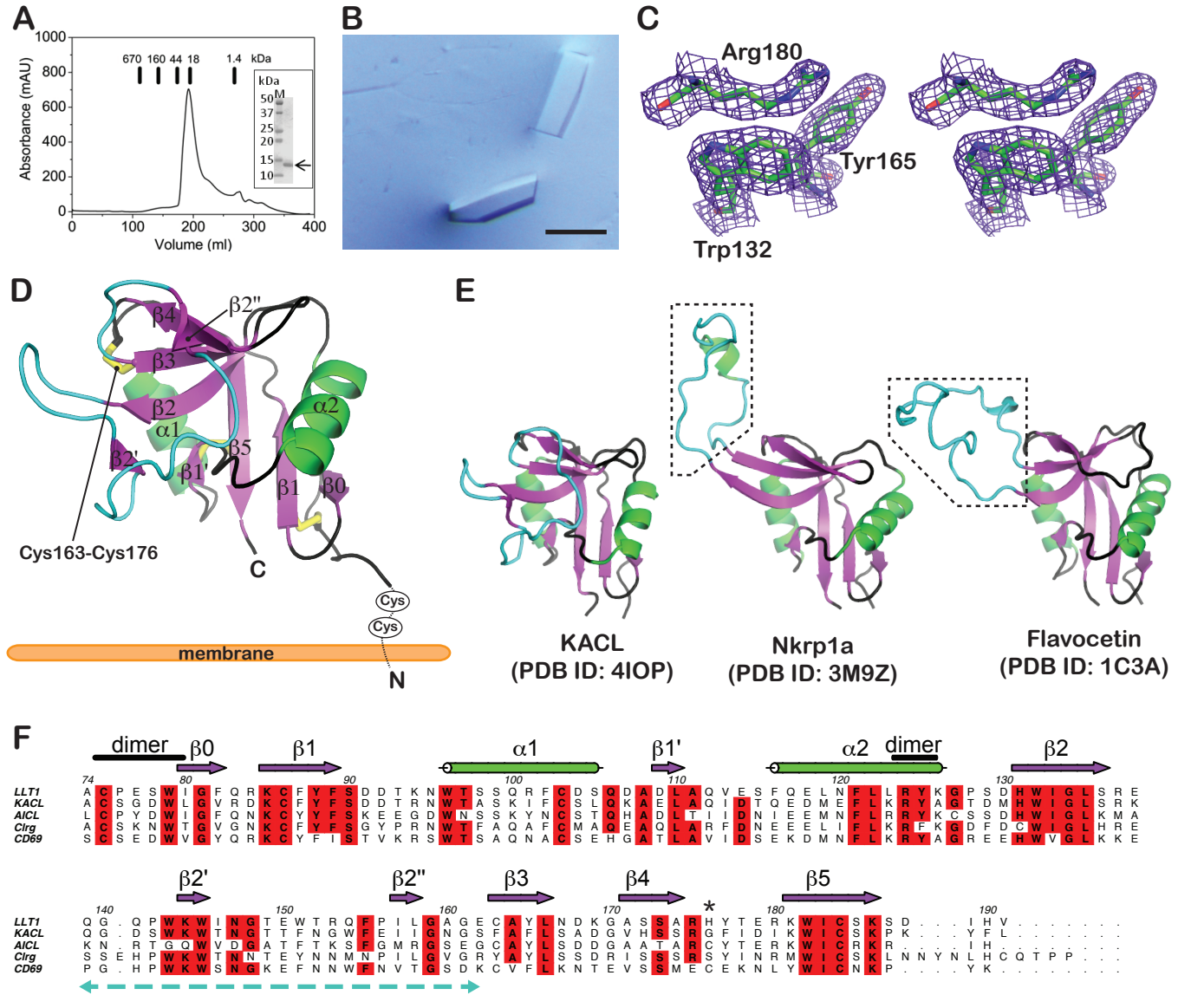
A
Absorbance (mAU)
Volume (ml)
670 160 44 18
1.4 kDa
kDa
M
50
37
25
20
15
10
B
C
Arg180
Tyr165
Trp132
D
β4'
β2''
β3
β2
α1
α2
β2'
β1'
β5
β1
β0
Cys163-Cys176
C
Cys
Cys
membrane
N
E
KACL
(PDB ID: 4IOP)
Nkrp1a
(PDB ID: 3M9Z)
Flavocetin
(PDB ID: 1C3A)
F
dimer
β0
β1
α1
β1'
α2
dimer
β2
β2'
β2''
β3
β4
β5
LLT1
KACL
AICL
Clrg
CD69

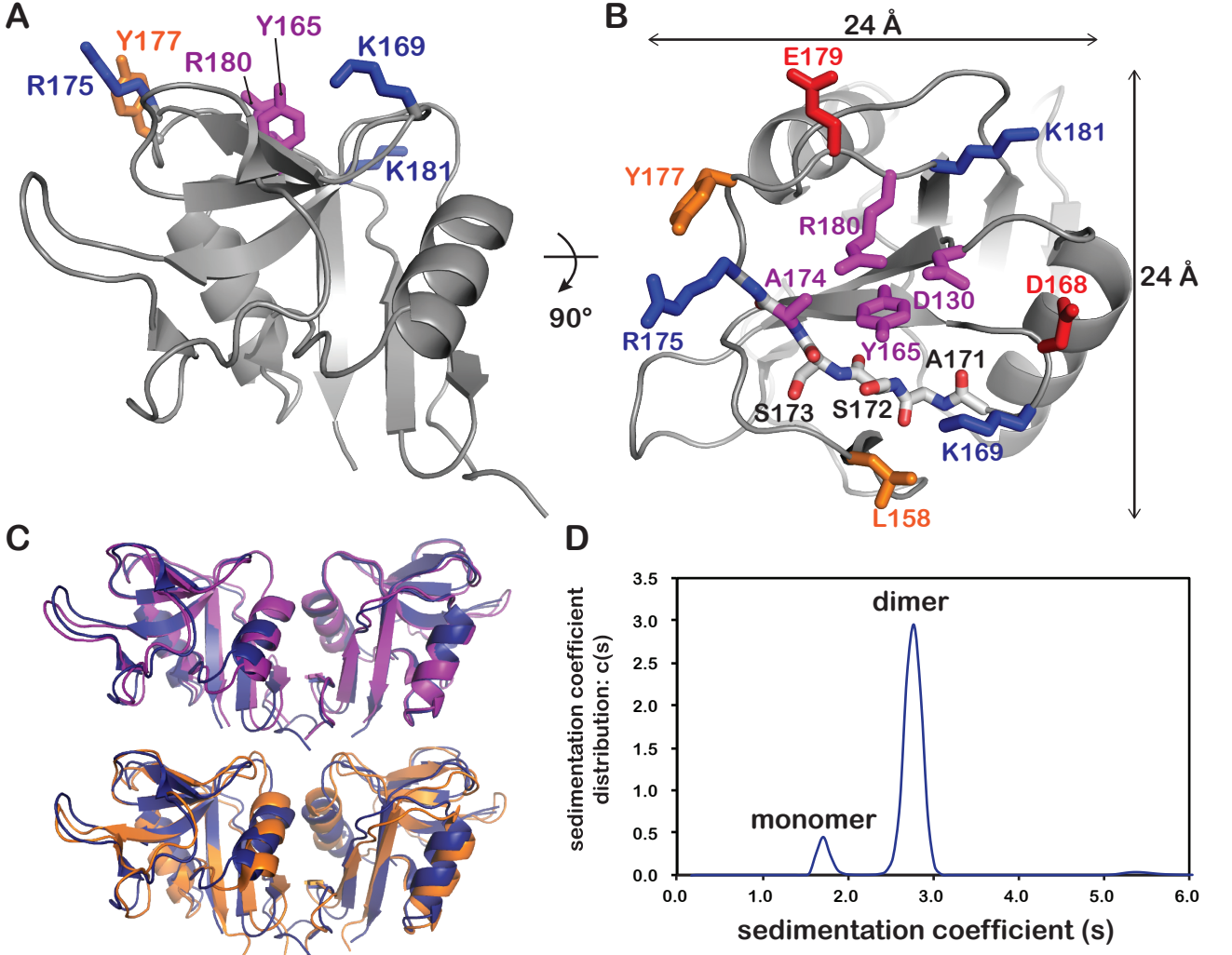
A
Y177
Y165
R180
K169
R175
K181
B
24 Å
E179
K181
Y177
R180
A174
D130
D168
24 Å
R175
Y165
A171
S173
S172
K169
L158
90°
C
D
dimer
monomer
sedimentation coefficient distribution: c(s)
sedimentation coefficient (s)
0.0
0.5
1.0
1.5
2.0
2.5
3.0
3.5
0.0
1.0
2.0
3.0
4.0
5.0
6.0

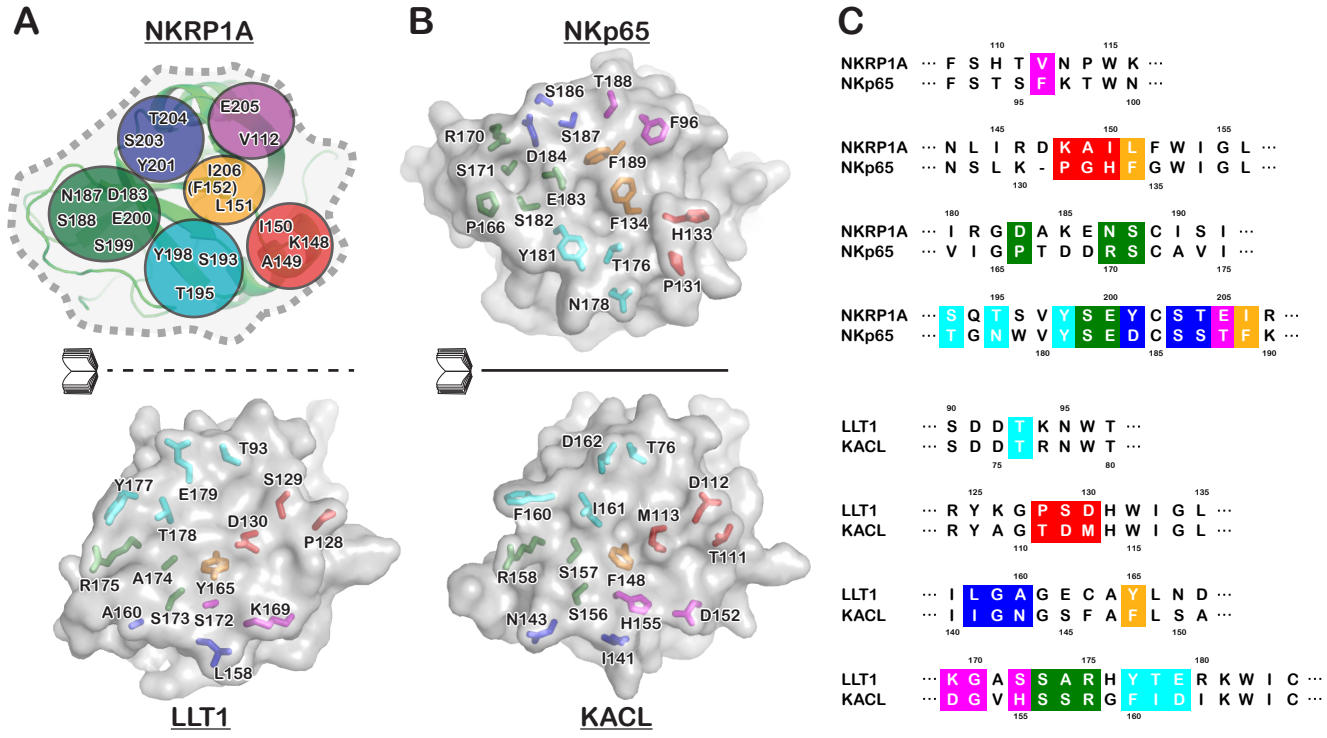
A
NKRP1A
T204
S203
Y201
E205
V112
I206
(F152)
L151
N187
D183
S188
E200
S199
Y198
S193
T195
I150
K148
A149
T93
Y177
E179
S129
D130
T178
P128
R175
A174
Y165
A160
S173
S172
K169
L158
LLT1
B
NKp65
T188
S186
F96
R170
S187
D184
S171
F189
E183
P166
S182
F134
H133
Y181
T176
P131
N178
D162
T76
D112
F160
I161
M113
T111
R158
S157
F148
N143
S156
H155
D152
I141
KACL
C
NKRP1A ··· F S H T V N P W K ···
NKp65 ··· F S T S F K T W N ···
NKRP1A ··· N L I R D K A I L F W I G L ···
NKp65 ··· N S L K - P G H F G W I G L ···
NKRP1A ··· I R G D A K E N S C I S I ···
NKp65 ··· V I G P T D D R S C A V I ···
NKRP1A ··· S Q T S V Y S E Y C S T E I R ···
NKp65 ··· T G N W V Y S E D C S S T F K ···
LLT1 ··· S D D T K N W T ···
KACL ··· S D D T R N W T ···
LLT1 ··· R Y K G P S D H W I G L ···
KACL ··· R Y A G T D M H W I G L ···
LLT1 ··· I L G A G E C A Y L N D ···
KACL ··· I I G N G S F A F L S A ···
LLT1 ··· K G A S S A R H Y T E R K W I C ···
KACL ··· D G V H S S R G F I D I K W I C ···

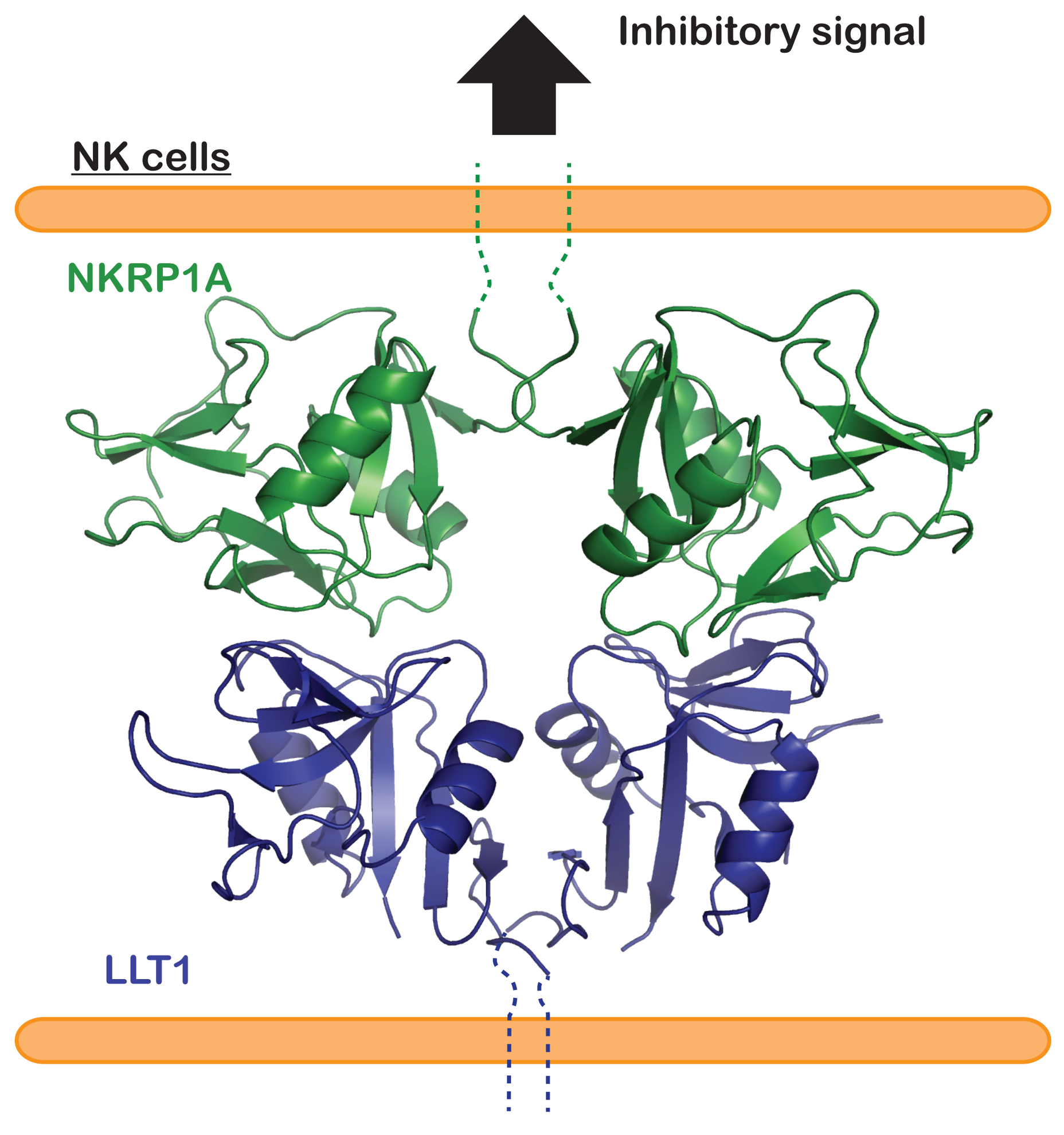
Inhibitory signal
NK cells
NKRP1A
LLT1